Journal of Solid State Chemistry 182 (2009) 2949–2960

Contents lists available at ScienceDirect

Journal of Solid State Chemistry

journal homepage: www.elsevier.com/locate/jssc

Structural characterization, thermal, dielectric, vibrational properties and molecular motions in $[C_3N_2H_5]_6[Bi_4Br_{18}]$

A. Piecha [a], R. Jakubas [a,*], A. Pietraszko [b], J. Baran [b], W. Medycki [c], D. Kruk [d]

[a] Faculty of Chemistry, University of Wrocław, Joliot-Curie 14, 50-383 Wrocław, Poland
[b] Institute of Low Temperature and Structure Research, PAS, Okólna 2, 50-950 Wrocław, Poland
[c] Institute of Molecular Physics, PAS, M. Smoluchowskiego 17, 60-179 Poznań, Poland
[d] Institute of Physics, Jagiellonian University, Reymonta 4, 30-059 Kraków, Poland

ARTICLE INFO

Article history:
Received 30 April 2009
Received in revised form
17 July 2009
Accepted 2 August 2009
Available online 12 August 2009

PACS:
61.05.C–
64.60.–i
65.40.–b
77.22.–d
78.30.–j
76.60.–k

Keywords:
Imidazolium
Bismuthate(III)
Phase transition
Dielectric relaxation
Infrared
^{1}H NMR

ABSTRACT

$[C_3N_2H_5]_6[Bi_4Br_{18}]$ has been synthesized and characterized by the X-ray (at 293 and 110 K), calorimetric, dilatometric and dielectric measurements. At room temperature it crystallizes in the monoclinic space group, $C2/m$. A crystal structure consists of disordered imidazolium cations and ordered discrete tetramers of $[Bi_4Br_{18}]^{6-}$. This compound reveals a rich polymorphism in a solid state. It undergoes three solid–solid phase transitions: from phase I to II at 426/423 K (heating–cooling), II→III at 227 K and III→IV at 219.5/219 K. A clear dielectric relaxation process is found in the room temperature phase **II**. Infrared studies of the polycrystalline $[C_3N_2H_5]_6[Bi_4Br_{18}]$ showed that the ν(N–H), δ(ring) and δ(C–H) modes of the imidazolium cations appeared to be very sensitive to the IV→III phase transition. ^{1}H NMR measurements confirmed a key role of the imidazolium cations in the phase transitions mechanisms at low temperatures.

1. Introduction

Halogenoantimonates(III) and halogenobismuthates(III) molecular–ionic complexes are well known for the ability of their anion moieties to exhibit a wide range of geometry, stoichiometry and connectivity. These salts with a general formula $R_aM_bX_{3b+a}$ (where R denotes an organic cation, M denotes Sb(III) or Bi(III) and X = Cl, Br, I) appear to crystallize in more than 30 different anionic structures [1]. The most interesting salts, having ferroic properties (ferroelastic and ferroelectric), are limited to those characterized by the chemical composition of $R_3M_2X_9$ [2–5] and $R_5M_2X_{11}$ [6–8]. Curiously enough, all known compounds of the $R_5M_2X_{11}$-type were found to exhibit ferroelectric properties. A characteristic feature of these salts is the presence of discrete bioctahedral anionic units $[M_2X_{11}]^{5-}$ comprising only one bridging halogen atom in the structure. In the case of $R_3M_2X_9$ four various anionic forms were discovered, where three out of six halogen atoms are terminal and the others are bridging. The MX_6 octahedra are able to form: (i) infinite one-dimensional chains, (ii) two-dimensional layers, (iii) discrete bioctahedral or (iv) discrete tetramer units $[M_4X_{18}]^{6-}$. It has turned out that salts crystallizing with a two-dimensional anionic substructure (type-(ii)) with small counterions, such as monomethyl-, dimethyl- and trimethyl-ammonium, have some tendency to exhibit ferroelectric properties. It has been proved that dynamics of the dipolar organic cations is responsible for a long-range order of the ferroelectric type in the $R_3M_2X_9$-type compounds.

In search for new polar crystals we extended our studies of halogenoantimonates(III) and halogenobismuthates(III) incorporating relatively small aromatic nonsubstituted pentagonal cations e.g. imidazolium and pyrazolium into the crystal structure. Quite recently we have succeeded in obtaining several ferroelectric ionic compounds of the halogenoantimonates(III) and halogenobismuthates(III) families, with an imidazolium counterion, characterized by the chemical stoichiometry $R_5M_2X_{11}$ [9–11]. Apart from this type of compounds, solid ionic complexes containing the

* Corresponding author. Fax: +48 713282228.
E-mail address: rj@wchuwr.chem.uni.wroc.pl (R. Jakubas).

0022-4596/$ - see front matter © 2009 Elsevier Inc. All rights reserved.
doi:10.1016/j.jssc.2009.08.007

imidazolium cations have some tendency to crystallize with the composition of $R_6M_4X_{18}$, which are characterized by the presence of discrete anionic tetramer $[M_4X_{18}]^{6-}$. Interestingly enough, the $R_6M_4X_{18}$ composition occur extremely rarely in halogenoantimonates(III) and halogenobismuthates(III) and only several examples of such a type of compounds have been known so far; $[C_5H_5NH]_6[Bi_4Cl_{18}]$ [12] and $[C_3N_2H_5]_6[Bi_4Cl_{18}]$ [13]. Recently, we have synthesized an innovative derivative crystallizing with the following stoichiometry: $[C_3N_2H_5]_6[Bi_4Br_{18}]$.

In this paper the results of the studies of the crystal structure (single-crystal X-ray and powder X-ray diffraction), thermal (differential scanning calorimetry, TGA, dilatometry), dielectric and vibrational properties of $[C_3N_2H_5]_6[Bi_4Br_{18}]$ are described. Molecular motion of the imidazolium cations were studied by means of proton magnetic resonance (^{1}H NMR). A possible mechanism of the phase transitions in the title compound is discussed.

2. Experimental

The starting materials for the synthesis of the imidazolium bromobismuthate(III), $[C_3N_2H_5]_6[Bi_4Br_{18}]$, were commercial $BiBr_3$ (99.999%, Aldrich), imidazole amine—$C_3N_2H_4$ (99.5%, Fluka)—and HBr (48%, Sigma-Aldrich). An aqueous solution of the imidazolium bromide was added to a solution of the bismuth oxide (Bi_2O_3) in 48% aqueous of hydrobromic acid. The resulting yellow precipitate was redissolved by heating and on cooling gave dark yellow polycrystals. Analysis: found: C—8.02%, N—6.21%, H—1.16%; (calc., C—8.04%, N—6.25%, H—1.12%). Single crystals were grown from an aqueous solution by slow evaporation at constant room temperature of 300 K.

Differential scanning calorimetry (DSC) was recorded using a Perkin Elmer DSC-7 in the temperature range of 100–450 K.

The dilatometric measurements were performed by a thermomechanical analyzer Perkin Elmer TMA-7 in the temperature range of 100–450 K. The dimensions of the sample were of the order of $3 \times 2 \times 1\,mm^3$.

Complex electric permittivity $\varepsilon^* = \varepsilon' - i\varepsilon''$ was measured between 100 and 450 K by an Agilent 4284A Precision LCR Meter in the frequency range between 100 Hz and 1 MHz. The dimensions of the sample were approximately of $4 \times 4 \times 1\,mm^3$. The overall error was less than 5%.

Infrared spectra of the $[C_3N_2H_5]_6[Bi_4Br_{18}]$ crystal (mulls in Nujol and in Fluorolube (only in room temperature)) in the temperature range of 10–300 K were recorded with a BRUKER IFS-88 spectrometer over the wavenumber range of $4000-400\,cm^{-1}$ with the resolution of $0.5\,cm^{-1}$. APD Cryogenics Displex closed cycle helium cryogenic refrigeration system (Model CSW-202) was used for temperature-dependent studies. Temperature of the sample was maintained at an accuracy of ± 0.1 K. Powder FT-Raman spectra were recorded with a FRA-106 attachment to the Bruker IFS-88 using Nd:YAG diode pump laser. The measurements were performed over the wavenumber range of $3500-80\,cm^{-1}$ at room temperature with a resolution better than $2\,cm^{-1}$. A program GRAMS/386 Galactic Industries was used for numeral fitting of the experimental data.

Measurements of proton relaxation times T_1 were carried out over a wide temperature range, using a Bruker SXP pulse spectrometer operating at Larmor frequencies of 90 MHz, by means of $180^\circ-(\tau)-90^\circ$ pulse sequences for times less than 1 s and by a saturation recovery method for times longer than 1 s. For NMR experiments the sample was evacuated and sealed off.

The X-ray diffraction data were collected using an automatic X-ray four-circle KM4CCD diffractometer and an EXCALIBUR diffractometer with CCD area detectors. Graphite monochromated Mo-$K\alpha$ radiation ($\lambda = 0.071073$ nm) was generated at 50 kV and 25 mA. A single image for 1° rotation around the ω-axis was obtained during 30 s and a full set of X-ray diffraction in the 2Θ angle was collected over the range from 3° to 93°. Intensities of the reflections were recorded in 1200 frames. Data reduction was performed using CrysAlis version 171.31.18 (Oxford) system with an analytic absorption correction. Crystal structures were solved and refined using a system of SHELXL-97 programs [14].

Powder diffraction data from RT to 160 K were collected on the X'Pert PRO X-ray diffractometer with a PIXcel ultra-fast line detector, focusing mirror and Soller slits for Cu$K\alpha$ radiation. For measurement of the powder X-ray diffraction patterns of $[C_3N_2H_5]_6[Bi_4Br_{18}]$, a pure single crystal material was ground using a mortar and a pestle and loaded into a glass capillary (0.7 mm diameter).

Crystallographic data for the structure reported in this paper (excluding structure factors) have been deposited with the Cambridge Crystallographic Data Centre, CCDC numbers 627189 and 729103. Copies of this information may be obtained free of charge from the Director, CCDC, 12 UNION Road, Cambridge CB2 1EZ. UK (fax: +44 1223 336033; e-mail: deposit@ccdc.cam.ac.uk or http://www.ccdc.cam.ac.uk).

3. Results

3.1. Thermal properties (DSC, TGA)

In order to determine phase relations in $[C_3N_2H_5]_6[Bi_4Br_{18}]$, the differential scanning calorimetry (DSC) measurements have been undertaken. The DSC curves for the $[C_3N_2H_5]_6[Bi_4Br_{18}]$ crystal during cooling and heating scans of 5 K/min are presented in Fig. 1. A phase situation in the compound under investigation seems to be quite complex since it depends on the thermal history of the sample as

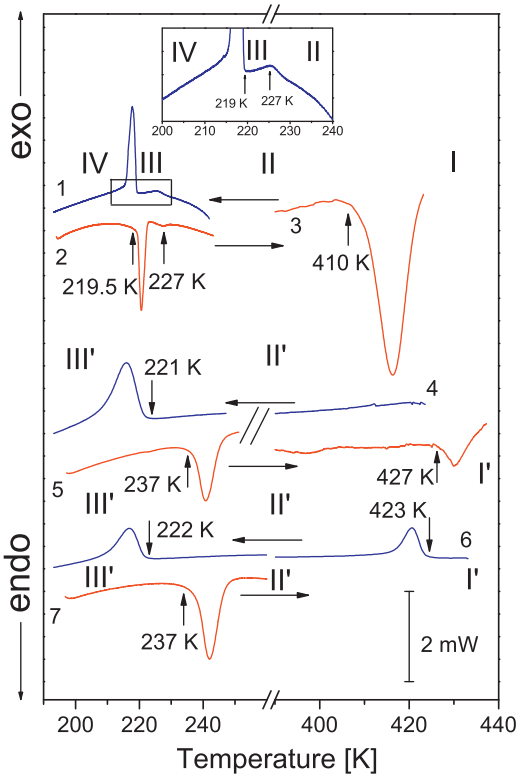

Fig. 1. DSC curves of $[C_3N_2H_5]_6[Bi_4Br_{18}]$ obtained on cooling and heating at the scanning rate of 5 K/min (sample mass −11.2 mg).

well. Fig. 1 indicates clearly that below room temperature (scans 1 and 2) the compound undergoes two closely laying reversible phase transitions (PTs); at 227 K second-order type (from phases **II** to **III**) and at 219.0/219.5 K (cooling–heating) first-order (from phases **III** to **IV**). The later PT is accompanied by a relatively small temperature hysteresis ($\Delta T = 0.5$ K) but discontinuous character of this transition was confirmed by the presence of the phase front observed on a single crystal sample under the polarizing microscope. The III→IV PT is accompanied by the transition entropy ca. $\Delta S = 39 \pm 4$ J/mol K. Heating of the compound above room temperature (scan 3) leads to the strong first order PT (II→I) at ca. 410 K accompanied by a huge entropy effect; $\Delta S = 79 \pm 8$ J/mol K. The sample was warmed up to 425 K and during the next cooling cycle (scan 4) no thermal anomaly corresponding to the 410 K PT was observed down to room temperature (RT). Further cooling below RT reveals a low temperature reversible anomaly which corresponds, most likely, to the previous PT III→IV (scans 4 and 5). Unexpectedly, this PT (221/237 K) is now accompanied by a significant temperature hysteresis ca. 16 K and $\Delta S = 52 \pm 5$ J/mol K. Above RT (scan 5) the compound undergoes reversible first order PT at 427/423 K (heating–cooling) with $\Delta S = 16 \pm 2$ J/mol K. In the low temperature region (scans 6 and 7) a phase situation is stable and the PT II′→III′ appears at the same temperature as that seen on the curve of the scans 4 and 5. Taking the entropy transition magnitudes into account all the first-order PTs may be classified as an "order–disorder".

Fig. 2 shows a simultaneous thermogravimetric analysis (TGA) and a differential thermal analysis (DTA) scan for the $[C_3N_2H_5]_6[Bi_4Br_{18}]$ crystal between 300 and 700 K. A large endotherm at ca. 410 K corresponds to the structural PT detected by DSC and it is accompanied by negligible weight loss of the sample. The compound seems to be stable up to about 520–540 K. Further heating brings about continuous and pronounced decomposition of the sample. The first order character of the phase transition at 410 K was confirmed by the linear thermal expansion measurements (see Part A in the supplementary material).

A smarter presentation of the thermal expansion of $[C_3N_2H_5]_6[Bi_4Br_{18}]$ below RT in comparison to that estimated by a linear thermal expansion method (TMA) results from the powder X-ray diffraction measurements carried out from RT down to 160 K. Temperature dependencies on lattice parameters *a*, *b* and *c* and a monoclinic β angle and a volume of the unit cell are shown in Fig. 3. The most significant changes, on cooling, were found along the *c*- and *a*-axes, with expansion of about 0.9% and compression of about 2.2%, respectively. It should be emphasized that a structural anomaly for the *a*-direction is relatively large which justifies strong distortion of the lattice cell and breakage of a single crystal. A thermal anomaly along the *b*-direction is characterized by some distribution of the experimental points in the close vicinity of II→III and III→IV PTs, however, a change in dilation for *b*-axis is significantly smaller than those for the remaining directions. Similarly, any changes in the β angle in this temperature region are rather subtle. This transition also leads to a positive change in the crystal lattice volume by ca. 0.9%. A pressure coefficient for this first-order phase transition is estimated from the Clausius–Clapeyron relation:

$$\frac{dT_c}{dp} = \frac{\Delta V}{\Delta S} \quad (1)$$

where $\Delta V/V = 1.2 \times 10^{-2}$ is a change in the molar volume and ΔS is a magnitude of the transition entropy (39 J/mol K). The pressure coefficient for the phase transition at 219 K (upon cooling) is found to be about 0.3 K MPa^{-1}.

Summarizing the results of the dilatometric measurements one can state that the main distortion of the crystal structure at low temperatures (II→III and III→IV PTs) takes place within the *ac*-plane.

3.2. X-ray diffraction studies

A single crystal X-ray diffraction examination of $[C_3N_2H_5]_6[Bi_4Br_{18}]$ at 420 K showed that reflections after the transformation from phases **II** to **I** were very weak and smeared. The collected data at 420 K were not sufficiently good for crystal structure determination. Crystal structures have been determined in phase **II** at 293 K and in phase **IV** at 110 K. The first order phase transition from phases **II** to **III** is coupling with very large distortion of the unit cell and a diffraction pattern in the vicinity of the transition surrenders to the worsening. For this reason any determination of the symmetry and a crystal structure of the intermediate phase **III** was omitted. An examination of the symmetry of the phases **II** and **IV** revealed that both of them belong to the monoclinic space group, *C*2/*m*.

The analyzed crystal appears to be isomorphous to known halogenobismuthate(III) derivatives characterized by the $[M_4X_{18}]^{6-}$ anionic form, which crystallize in their disordered phases in the monoclinic space group *C*2/*m*; ($[C_5H_5NH]_6[Bi_4Cl_{18}]$

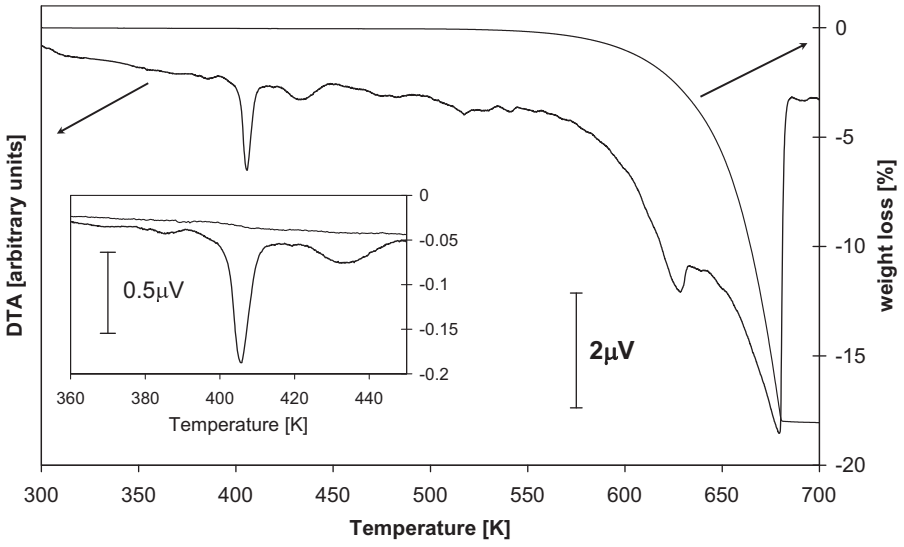

Fig. 2. Simultaneous thermogravimetric analysis (TGA) and differential thermal analysis (DTA) scan for the $[C_3N_2H_5]_6[Bi_4Br_{18}]$ crystal.

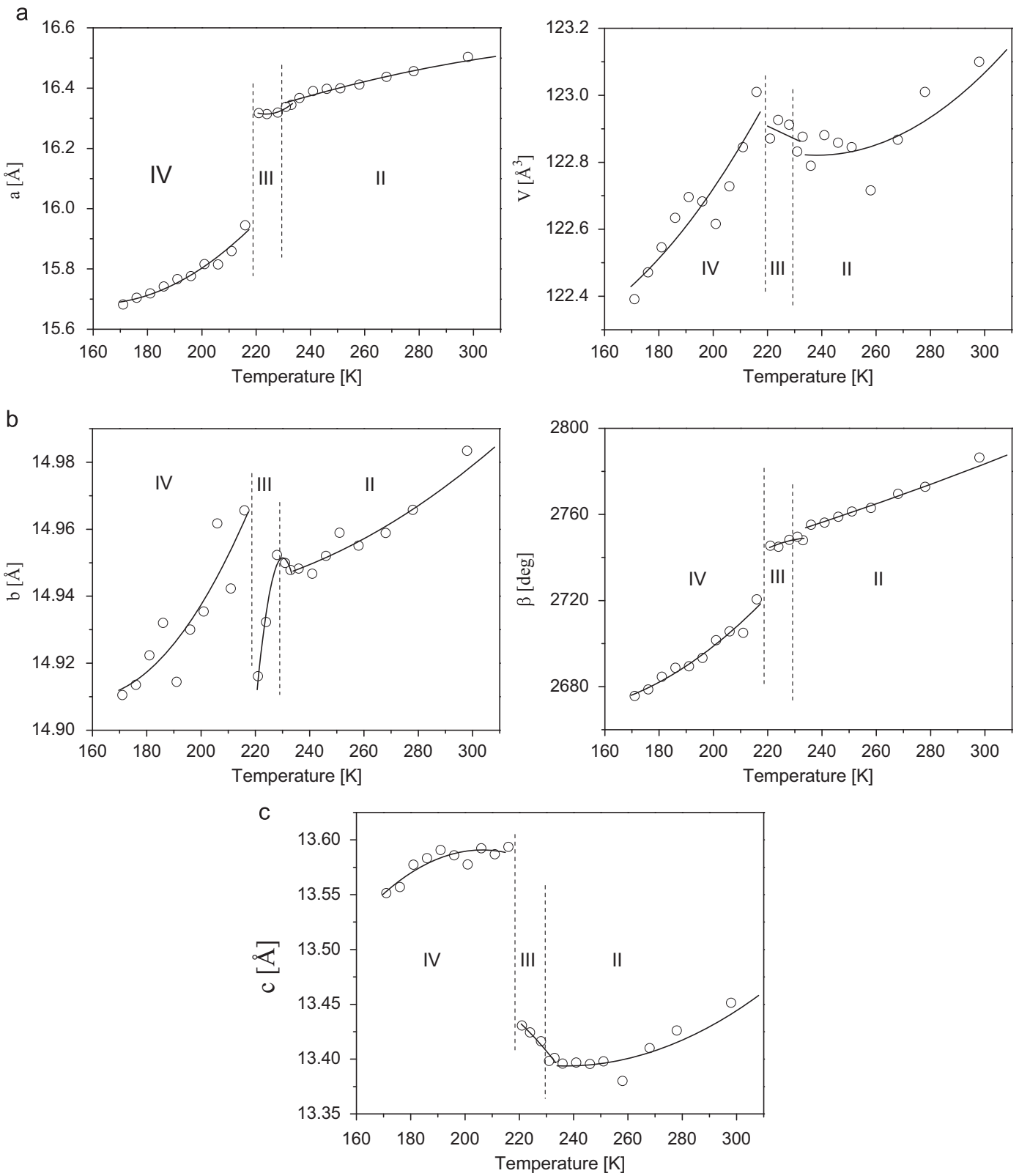

Fig. 3. Experimental values of the lattice parameters *a*, *b*, *c*, the *β* monoclinic angle and volume of the unit cell (*V*) as a function of temperature for $[C_3N_2H_5]_6[Bi_4Br_{18}]$ obtained from the powder X-ray diffraction measurements.

[12] and $[C_3N_2H_5]_6[Bi_4Cl_{18}]$ [13]). Crystallographic data and details on the structure determination of $[C_3N_2H_5]_6[Bi_4Br_{18}]$ are given in Table 1. The structural parameters (selected bond lengths and angles) resulting from the analysis of these data are available in the supplementary material (Part B). The structure of octahedron unit with three nonequivalent imidazolium cations and the atomic numbering scheme is presented in Fig. 4. A discrete unit $[Bi_4Br_{18}]^{6-}$ consists of two pairs of edge-sharing octahedrons connected by bromine ligands (Br5 and Br2). Anionic moieties are centered about the crystallographic points 0,1/2,1/2; 1/2,0,1/2

Table 1
Crystal data and structure refinement for $[C_3N_2H_5]_6[Bi_4Br_{18}]$ at 293 and 110 K.

	$[C_3N_2H_5]_6[Bi_4Br_{18}]$	
Crystal data		
Temperature (K)	293	110
Formula weight ($g\,mol^{-1}$)	2688.84	2688.84
Crystal system, space group	Monoclinic, $C2/m$	Monoclinic, $C2/m$
a (Å)	16.479(1)	15.495(3)
b (Å)	14.974(2)	14.807(3)
c (Å)	13.443(1)	13.428(3)
β(°)	123.00(1)	122.27(3)
V (A^3)	2782.0(4)	2605.1(9)
Z	2	2
D_{calc} ($g\,cm^{-3}$)	3.210	3.428
μ (mm^{-1})	25.569	27.305
F(000)	2368	2368
Crystal size (mm)	0.38 × 0.28 × 0.21	0.38 × 0.34 × 0.27
Data collection		
Diffractometer	Kuma KM4 diffractometer with CCD area detector	
Monochromator	graphite	graphite
Radiation type, wavelength, λ (A)	MoKα, 0.71073	MoKα, 0.71073
Θ range (deg)	3.19–28.16	3.26–28.52
Indeks range	$-21 \le h \le 21$	$-20 \le h \le 20$
	$-18 \le k \le 19$	$-19 \le k \le 19$
	$-17 \le l \le 17$	$-17 \le l \le 16$
Absorption correction	Numerical	
T_{min}/T_{max}	0.0093/0.1015	
Measured reflections	13 044	13 225
Independent reflections	3320	3244
R_{int}	0.00858	0.0744
Refinement		
Data/restraints/parameters	3320/3/137	3244/0/125
$R(F_0^2 > 2\sigma(F_0^2))$	$R_1 = 0.0456$	$R_1 = 0.0504$
	$wR_2 = 0.0832$	$wR_2 = 0.0900$
R(all data)	$R_1 = 0.0817$	$R_1 = 0.0881$
	$wR_2 = 0.0927$	$wR_2 = 0.0950$
$GooF = S$	1.019	1.358
$\Delta\rho_{max}/\Delta\rho_{min}$ (eA^{-3})	1.697/ − 1.823	3.360/ − 2.296

which agrees with the Wyckoff position 2(d) in the space group $C2/m$. It leads to the point symmetry C_{2h} of the whole tetramer $[Bi_4Br_{18}]^{6-}$.

Bridging and terminal bromine atoms are ordered at room temperature. Imidazolium cations are connected with the $[Bi_4Br_{18}]^{6-}$ moieties by relatively weak and significantly nonlinear N−H···Br hydrogen bonds (Table 2). The shortest N(1B)−H(1B)···Br(4) hydrogen bond with the length of ca. 3.7 Å and an angle close to 144° indicates extremely weak hydrogen bond system in the crystal under investigation. The remaining hydrogen bonds are significantly nonlinear. One can conclude that all the $[M_4X_{18}]$-tetramers are practically undistorted because interactions between organic cations and an anionic substructure are rather faint. Thus, in the case of the $[C_3N_2H_5]_6[Bi_4Br_{18}]$ analog imidazolium cations are able to perform quite free reorientational motion in the room temperature phase **II**.

Figs. 5a and b show projections of the crystals structure along the *b*-axis. The comparison of the crystal structure of the phase **II** and the phase **IV** proves that the arrangement of the anionic substructure ($[Bi_4Br_{18}]^{6-}$) does not experience any noticeable changes. On the other hand dramatic changes in the orientation of the imidazole rings take place. Both in the phases **II** and **IV** all the planes of the imidazole rings are perpendicular to the *ac*-plane (parallel to the *b*-axis). In the phase **II** three types of cations are oriented at various angles with respect to the OK1 plane. Significant displacement factors for all the C and N atoms of the imidazolium cation in the RT phase **II** may be explained in terms of the possible dynamical disorder. Any attempts at splitting their positions were not successful. Nevertheless, one can suggest that cations are able to perform wide-angle libration or jumps

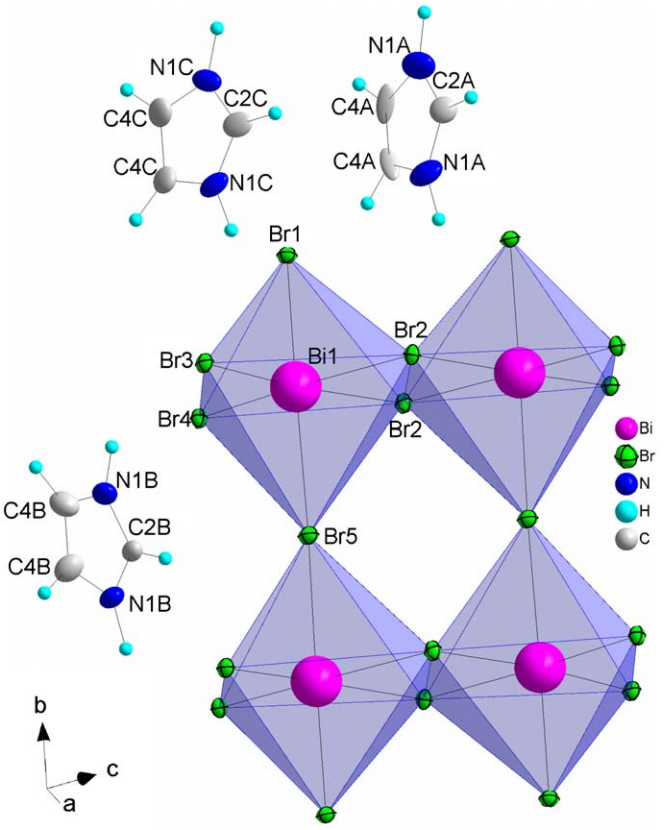

Fig. 4. Independent part of the unit cell of $[C_3N_2H_5]_6[Bi_4Br_{18}]$ at 110 K with the atom labeling scheme. Displacement ellipsoids are shown at the 50% probability.

between at least the two positions with relatively small activation energy for these motions. In the phase **IV** the plane of the imidazole rings N1B is parallel to $(2\,0\,\bar{1})$ plane. Rings of the remaining cations (N1A and N1C) are almost parallel to *bc*-plane. The observed structural changes suggest that through the phase transition III→IV we deal not only with diminishing freedom of the cations motion within the pentagonal ring, but with dramatic shift/deflection of all rings with respect to the OK1 plane (see Fig. 6). Such an arrangement of the imidazole rings leads to very large distortion of the lattice parameters; *a* and *c* (see Fig. 3). During the phase transition from the phase **II** to the phase **IV** there is also observed a significant change in the hydrogen bonds configuration of the N−H···Br and C−H···Br types (see Table 2). Most of the hydrogen bonds contract in the phase **IV** by about 0.20–0.25 Å in comparison with those in the phase **II**, which affect freedom of the cations motion.

It seems to be interesting to compare the two closely related anionic tetramers of halobismuthates(III) in two compounds characterized by different chemical stoichiometries. The ferrocenium analog; $[(\eta^5 - C_5H_5)_2Fe]_4Bi_4Br_{16}$ was found to be the first example of the polybromobismuthate(III) compound consisting of a cluster of four edge-sharing distorted $BiBr_6$ octahedra [15]. A coordination sphere for one Bi atom consists of four bridging and two terminal bromine atoms, whereas the environment of the other Bi atom consists of three bridging and three terminal bromine atoms. It should be emphasized that the other environment of halogen atoms around the central metal atoms of the anionic unit is encountered quite rarely. In the case of the title compound, $[C_3N_2H_5]_6[Bi_4Br_{18}]$, all four Bi atoms possess three terminal and three bridging halogen atoms. Such a type of the environment is only characteristic for the compounds characterized by the $R_3M_2X_9$ stoichiometry (formally also $R_6M_4X_{18}$).

Table 2
Hydrogen bonds for $[C_3N_2H_5]_6[Bi_4Br_{18}]$.

D–H···A	d(D–H)	d(H···A)	d(D···A)	<(DHA)
293 K				
N(1B)–H(1B)···Br(4)	1.05(5)	2.81(6)	3.715(5)	144(8)
N(1A)–H(1A1)···Br(3)^{iv}	1.00(4)	3.11(7)	3.726(7)	121(5)
N(1A)–H(1A1)···Br(2)	1.00(4)	3.02(6)	3.710(5)	127(5)
N(1A)–H(1A1)···Br(2)^{v}	1.00(4)	3.02(5)	3.616(6)	119(4)
N(1A)–H(1A1)···Br(3)^{iv}	1.00(4)	3.11(7)	3.726(7)	121(5)
N(1C)–H(1C1)···Br(3)^{iv}	1.02(4)	3.06(5)	3.767(6)	127(4)
N(1C)–H(1C1)···Br(4)	1.02(4)	3.05(7)	3.669(6)	120(6)
iv : $x+1/2,-y+1/2,z$; v : $-x+3/2,-y+1/2,-z+1$; vi : $-x+1/2,-y+1/2,-z$.				
110 K				
N(1B)–H(1B)···Br(4)	1.05	2.73	3.563(6)	136.4
N(1B)–H(1B)···Br(4)^{vi}	1.05	2.71	3.447(5)	127.5
N(1A)–H(1A1)···Br(2)^{viii}	1.05	2.91	3.632(6)	126.5
N(1A)–H(1A1)···Br(3)^{i}	1.05	2.68	3.432(7)	128.0
N(1C)–H(1C1)···Br(3)^{iii}	1.05	2.85	3.562(6)	125.2
N(1C)–H(1C1)···Br(2)	1.05	2.70	3.467(6)	129.6
i : $-x+1,y,-z+1$; iii : $x+1/2,-y+1/2,z$; vi : $-x+1/2,-y+1/2,-z$.				
viii : $-x+3/2,-y+1/2,-z+1/2$.				

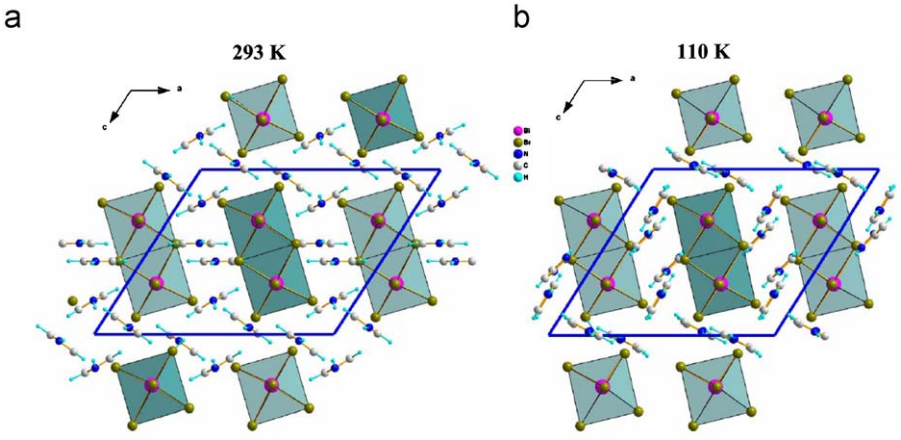

Fig. 5. The projection of the crystal structure along the *b*-axis for the phases **II** and **IV**.

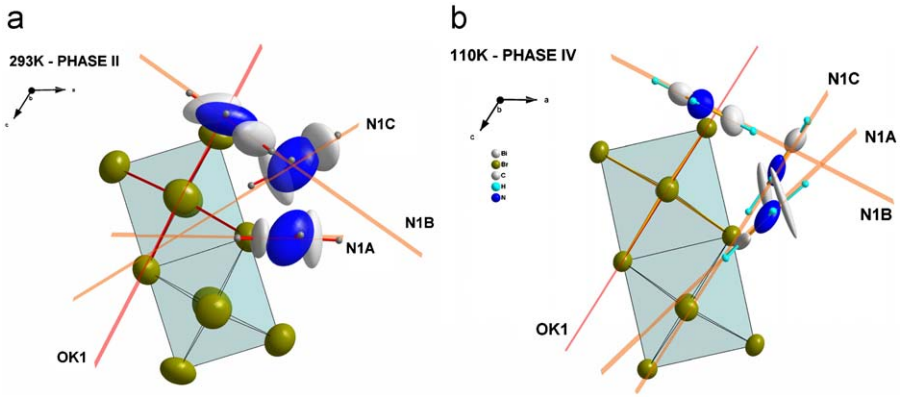

Fig. 6. The view of the selected fragment of the crystal structure at 298 K (phase **II**) and 110 K (phase **IV**) with the pronounced plane of imidazole rings and the plane OK1 created by the atoms Br1, Br2, Bi1, Br4 and Br5.

Fig. 7 presents powder diagrams of $[C_3N_2H_5]_6[Bi_4Br_{18}]$ for the selected 2Θ positions for the temperature region 243–198 K covering the PTs II→III and III→IV. It is clearly seen that the intensity of (400) Bragg peak of the phase **II** below 225 K rapidly decreases and the shape of this diffraction peak drastically changes. Similarly the (132) peak which is characteristic of the phase **II** significantly decreases its intensity in the same temperature region. The behavior of these diffraction peaks may reflect the presence of the II→III PT. In turn, the Bragg peak $(2\,0\,\bar{4})$ characteristic of the phase **IV** emerges below 216 K. It should be noticed that the Bragg peak (400) present in the phases **II** and **IV** experiences a drastic shift by ca. 0.7°. Summarizing, the powder X-ray studies showed that the most qualitative changes take place between 225 and 216 K. For this narrow temperature region we

probably deal with an intermediate phase **III** which may be treated as a coexistence of two phases: **II** and **IV**.

3.3. Dielectric properties

Temperature dependencies of the complex electric permittivity, ε^*, of $[C_3N_2H_5]_6[Bi_4Br_{18}]$ were measured along the main crystallographic directions over the temperature range of 100–450 K for the kilohertz frequency region. The temperature dependence of ε' below room temperature at selected frequencies between 2 kHz and 1 MHz measured along the *a*-axis is shown in Fig. 8a. Two steps on the ε'_a versus temperature curve are clearly visible. The rapid jump in the ε'_a value near T_c (II→III) is preceded by a small anomaly by several degrees. The lower temperature dielectric anomaly confirms the first-order character of the PT III→IV (dielectric characteristic for ε'_c(T) is quite similar), which is consistent with the DSC and dilatometric results. A dielectric increment ($\Delta\varepsilon'$) being of the order of 10 for the III→IV phase transition at 219 K is comparable for all crystallographic directions. A subtle dielectric anomaly at ca. 227 K corresponds to the II→III PT detected by DSC measurement. A dielectric increment in the vicinity of PT is weakly dependent on the frequency of the measuring electric field.

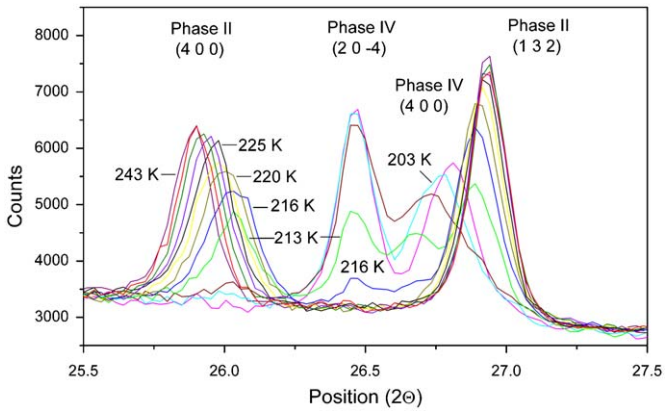

Fig. 7. Powder X-ray diffraction diagram of $[C_3N_2H_5]_6[Bi_4Br_{18}]$ for the selected Bragg peaks in the vicinity of II→III and III→IV PTs.

A clear relaxation process in the kilohertz frequency region 2 kHz–1 MHz is observed over the phase **II**. Fig. 8b shows temperature dependencies of the imaginary part of the complex electric permittivity (ε''). It has been found that the dielectric response over the phase **II** is well described by the Cole–Cole relation:

$$\varepsilon^* = \varepsilon_\infty + \frac{\varepsilon_0 - \varepsilon_\infty}{1 + (i\omega\tau)^{1-\alpha}} \quad (2)$$

where ε_0 and ε_∞ are the low and high frequency limits of the electric permittivity, respectively, ω is angular frequency, τ is the macroscopic relaxation time. The Cole–Cole diagrams at selected temperatures (between 230 and 260 K) are presented in Fig. 9.

It should be also perceived that a small asymmetry visible at the high frequency end of the Cole–Cole plots suggests a possibility of appearance of an additional higher frequency relaxator. On the other hand a significant deviation of the experimental points at the low frequency end of the Cole–Cole plots (below 8 kHz) is due to the strong conductivity contribution (defects of the sample) to the electric permittivity. These two—low and high frequency—contributions were not analyzed in detail in this paper.

It is seen that the Cole–Cole plots deviate from semi-circles at temperatures between 230 and 260 K (α ranges between 0.24 and 0.01) which means that over this temperature region the fundamental relaxation process changes its character from polydispersive to monodispersive. The experimental results were fitted with the Cole–Cole relation (Eq. (2)) at several temperatures. It is well known that for the nonferroelectric system (lack of

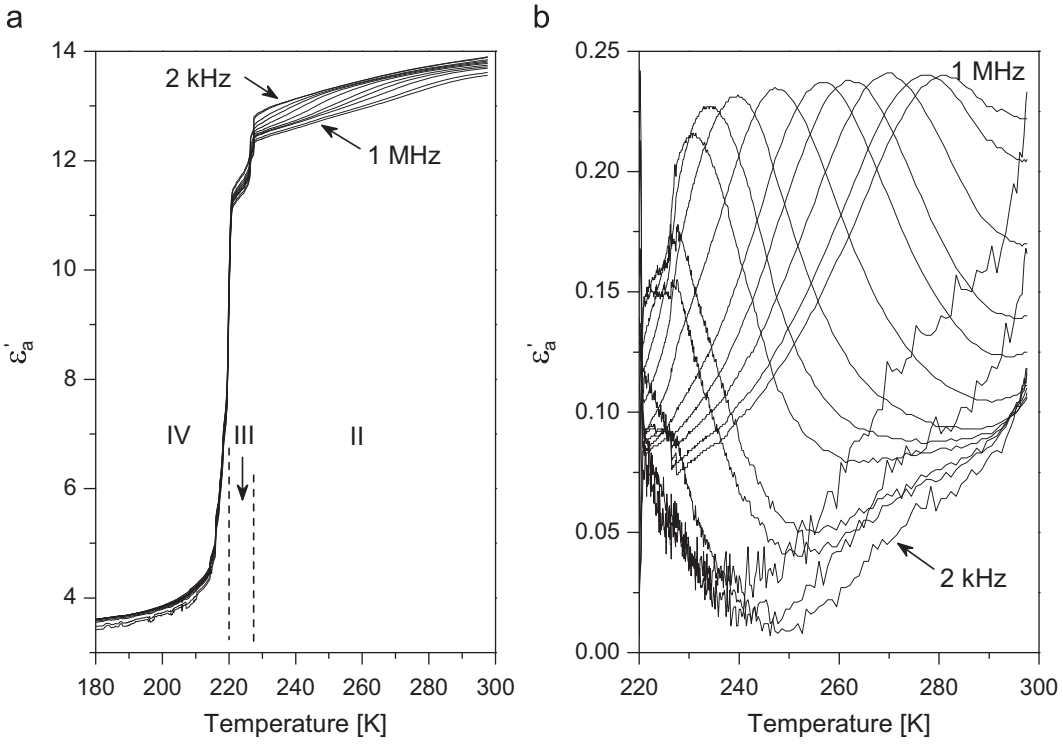

Fig. 8. Temperature dependence of the real (a) and imaginary (b) parts of complex dielectric permittivity along the *a*-direction at low temperatures.

long-range dipole–dipole interactions) the activation energy, E_a, can be estimated directly from the Arrhenius relation (Eq. (3)) (where τ is the macroscopic relaxation time):

$$\tau = C\exp\left(\frac{E_a}{kT}\right) \tag{3}$$

The activation energy E_a was found to be estimated at about 42 kJ/mol. Such a value is quite typical of bulky organic cations performing reorientational motion [16,17].

3.4. Infrared and Raman studies

Raman spectra at 300 K and IR spectra at 10 and 300 K are displayed in Fig. 10. The IR spectra in the frequency range 3000–2800, 1500–1330, and 750–700 cm^{-1} are characteristic of the Nujol bands. Thus, to cover these frequency regions we also measured the infrared spectrum of the $[C_3N_2H_5]_6[Bi_4Br_{18}]$ crystal in the Fluorolube mulls at 300 K.

The experimental IR frequencies at 10 and 300 K, Raman at 300 K and formal classification of the fundamental modes for the $[C_3N_2H_5]_6[Bi_4Br_{18}]$ crystal in the phases **II** and **IV** are collected in the supplementary material (Part C).

Formal classification of the fundamental ($k = 0$) modes predicts $16A_g + 15A_u + 14B_g + 15B_u$ modes for internal vibrations of the $[Bi_4Br_{18}]^{6-}$ anions and $39A_g + 33A_u + 33B_g + 39B_u$ modes for internal vibrations of the $(C_3N_2H_5)^+$ cations. The A_g and B_g type modes are Raman allowed, whereas the A_u and B_u are IR allowed.

The bands observed in 3500–400 cm^{-1} are due to the internal vibrations of the imidazolium cations, whereas the bands apparent below ca. 200 cm^{-1} are related to the internal vibrations of the $[Bi_4Br_{18}]^{6-}$ anions. The tentative assignment of the internal vibrations of the imidazolium cations is based on the previously reported vibrational studies on compounds containing the

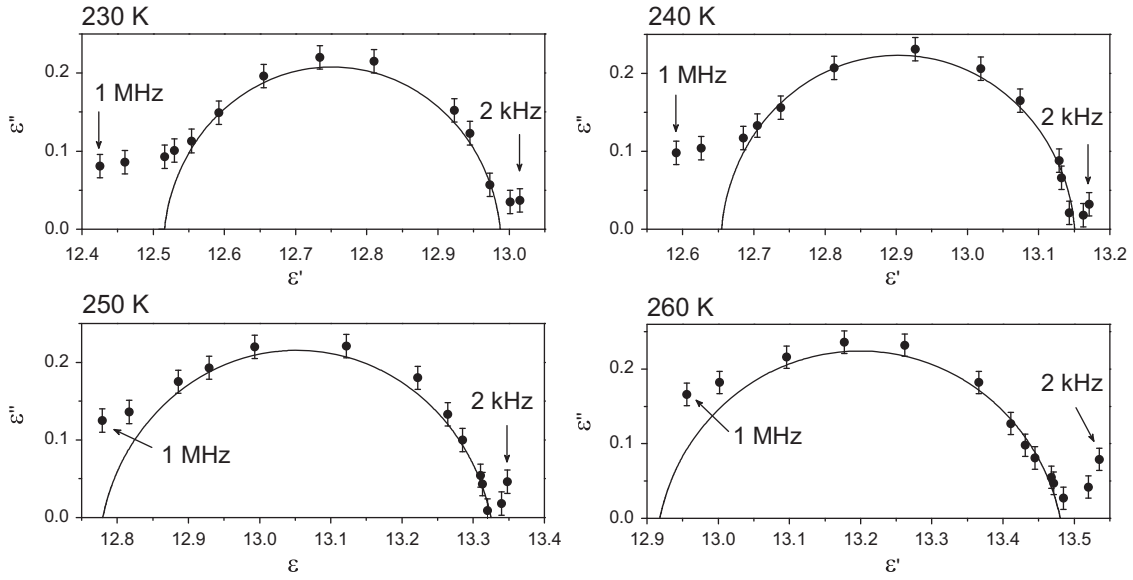

Fig. 9. Cole–Cole plots over the phase **II**.

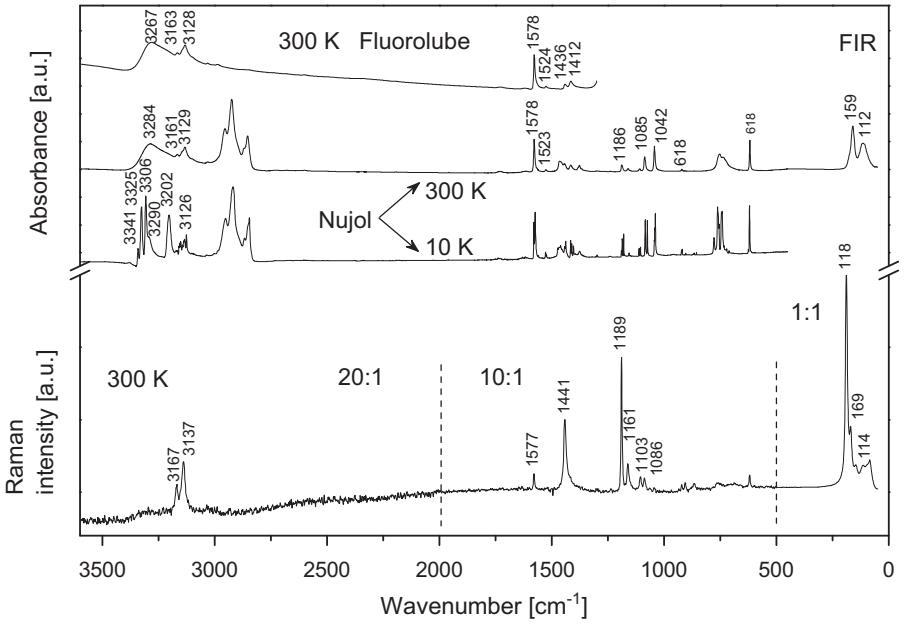

Fig. 10. Raman spectra at 300 K and IR spectra at 10 and 300 K for $[C_3N_2H_5]_6[Bi_4Br_{18}]$.

imidazole [18–22]. The assignments of the internal vibrations of the $[Bi_4Br_{18}]^{6-}$ anions are proposed on the basis of the results obtained for numerous bromobismuthates(III) derivatives [23–26].

The internal vibrations of the $[Bi_4Br_{18}]^{6-}$ *anions*: Intense Raman lines at 188 cm^{-1} clearly correspond to the symmetric Bi–Br stretching mode of the external bromines. In turn, intense infrared bands at 159 cm^{-1} (corresponding to weak Raman lines near 169 cm^{-1}) are due to the asymmetric Bi–Br stretching mode. Stretching frequencies for the bridged Bi–Br–Bi stretches give intense infrared absorption near 112 cm^{-1} and a rather weak Raman line near 114 cm^{-1}.

Temperature behavior of the internal vibrations of the imidazolium cations: The most spectacular temperature changes in the infrared spectra (in Nujol) were found for the modes in the frequency region between 3160 and 3360 cm^{-1}. The infrared spectrum measured at RT displays one broad band at ca. 3282 cm^{-1} attributable to the ν(N–H) vibration (see Fig. 11). In the spectrum measured at 10 K over this frequency region five bands appear, which may be explained by the presence of several nonequivalent (N–H) groups (at least six such groups are expected at the lowest temperature phase **IV**). It is clearly seen that a rapid splitting of the 3300 cm^{-1} mode takes place near the phase transitions IV→III and III→II.

The temperature evolution of the spectra for the wavenumber region 1175–1195 cm^{-1}, the FWHM of two modes (1180 and 1186 cm^{-1}) and the wavenumber positions of the modes assigned to the δ(ring) and δ(C−H) vibrations are shown in Figs. 12a, b and c, respectively. Any anomalies in the wavenumber positions at the phase transition temperature (219.5 K) of these modes are rather subtle, but a significant jump in their FWHM magnitudes is clearly seen.

The temperature evolution of the spectra between 1065 and 1095 cm^{-1} and the wavenumber positions of the 1074 and 1084 cm^{-1} modes assigned to the δ(C−H) vibrations are displayed in Figs. 13a and b. Both modes experience a clear jump in the wavenumber positions by ca. 6 and 3 cm^{-1}, respectively, close to 219.5 K.

It should be emphasized that most of the modes arising from ν(N−H), δ(ring) and δ(C−H) appeared to be very sensitive to the IV→III phase transition, confirming its discontinuous nature. We can conclude that a change in the motional state of the imidazolium cations is directly reflected in changes of the infrared spectra with temperature. Sudden freezing of the reorientational motion of $[C_3H_5N_2]^+$ takes place exactly at 219.5 K, which confirms the basic contribution of these cations to the mechanism of PT (III→IV).

3.4.1. Analysis of proton relaxation processes (^{1}H NMR)

Fig. 14 shows the log T_1 versus 1000/T over a wide temperature region. The ^{1}H NMR studies revealed a significant change in the activation energy of the proton motion through the 220 K PT (4 kJ/mol below 220 K and 10 kJ/mol above 220 K). It may be explained as a rapid release of the cationic motion after crossing the phase transition temperature (IV→III) on heating. We believed that it is due to the onset of reorientation of the imidazole pentagonal ring around its pseudo-five-fold axis.

Relaxation experiments performed at the magnetic field of 2.1 T (corresponding to the proton Larmor frequency of 90 MHz) show bi-exponential proton magnetization decays in a very broad temperature range. A simplified description (presented in the supplementary material—Part D) brings us to the conclusion that the bi-exponential proton relaxation below 220 K can be attributed to the H–Br dipole–dipole coupling and that the proton motion can be reasonably well represented as a process characterized by one correlation time.

Quite similar dynamics with respect to a motional state of the pentagonal aromatic cations was found in a case of the pyrazolium analog—$[C_3N_2H_5]_6Sb_4Br_{18}\cdot 2H_2O$ [27]. There were also two minima of the spine-lattice relaxation time (T_1)

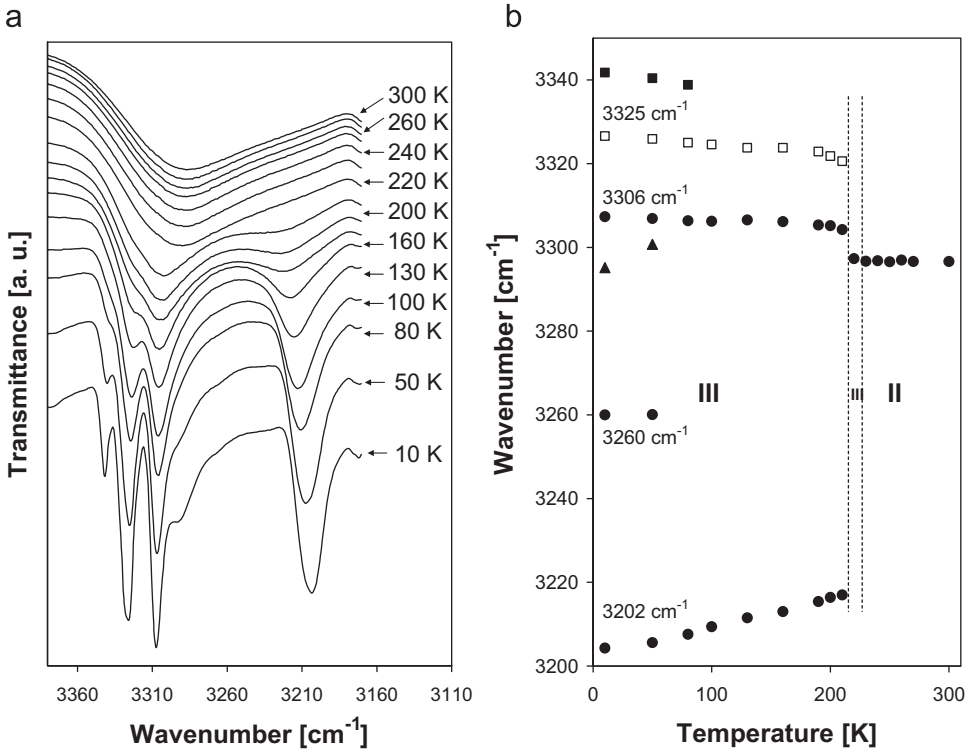

Fig. 11. (a) Temperature evolution of the NH stretching modes between 3160 and 3360 cm^{-1} and (b) temperature dependence of the wavenumbers of the bands assigned to the NH stretching modes.

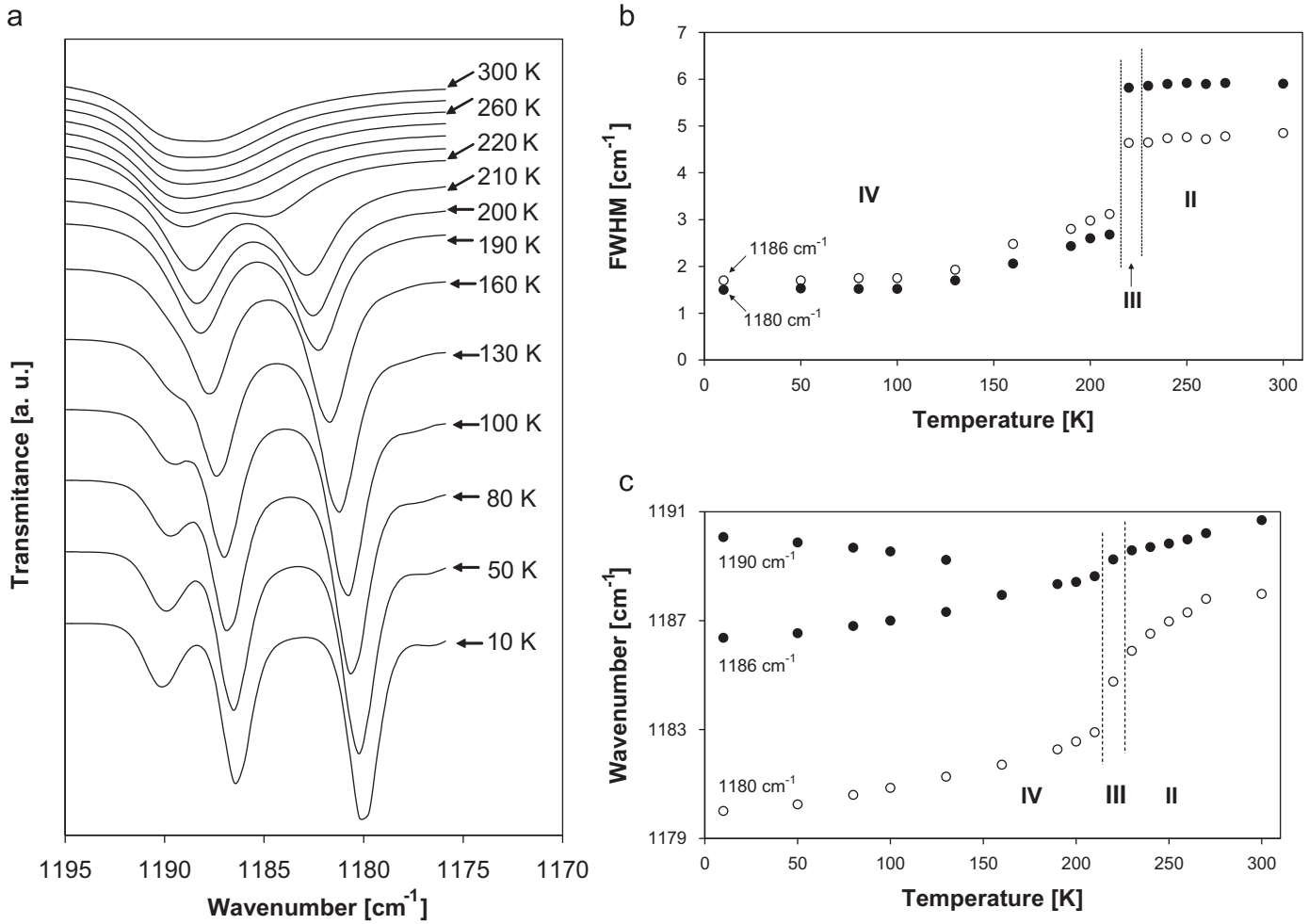

Fig. 12. (a) Temperature evolution of the IR spectra in the δ(ring) and δ(C−H) vibrations region (1175−1195 cm^{-1}), (b) the FWHM of two modes (1180 and 1186 cm^{-1}) and (c) the wavenumber positions of these modes between 10 and 300 K.

observed: at low temperatures a wide one attributed to a small-angle-libration of cations between the potential minima separated by an angle of ca. 13°, whereas the high temperature one assigned to the reorientation of a cation about its pseudo-five-fold axis. For the crystal under investigation, the interactions between the hydrogen and bromide nuclei modulate the quadrupole coupling which influences relaxation processes of protons, thus the analysis of the possible molecular motion seems to be complicated.

4. Discussion

So far, we have synthesized and characterized three organic-bismuthate(III) ionic connections crystallizing with a chemical composition of $R_6Bi_4X_{18}$ (X = Cl, Br) and containing aromatic cations (R) such as: imidazolium and pyridinium in the crystal structure. All these compounds appeared to be isomorphous in the room temperature phase-$C2/m$, nevertheless they revealed a different PT sequence at low temperatures:

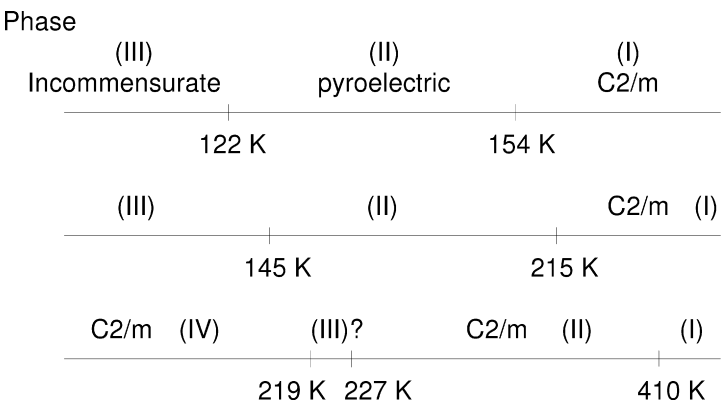

$[C_5NH_6]_6[Bi_4Cl_{18}]$

$[C_3N_2H_5]_6[Bi_4Cl_{18}]$

$[C_3N_2H_5]_6[Bi_4Br_{18}]$

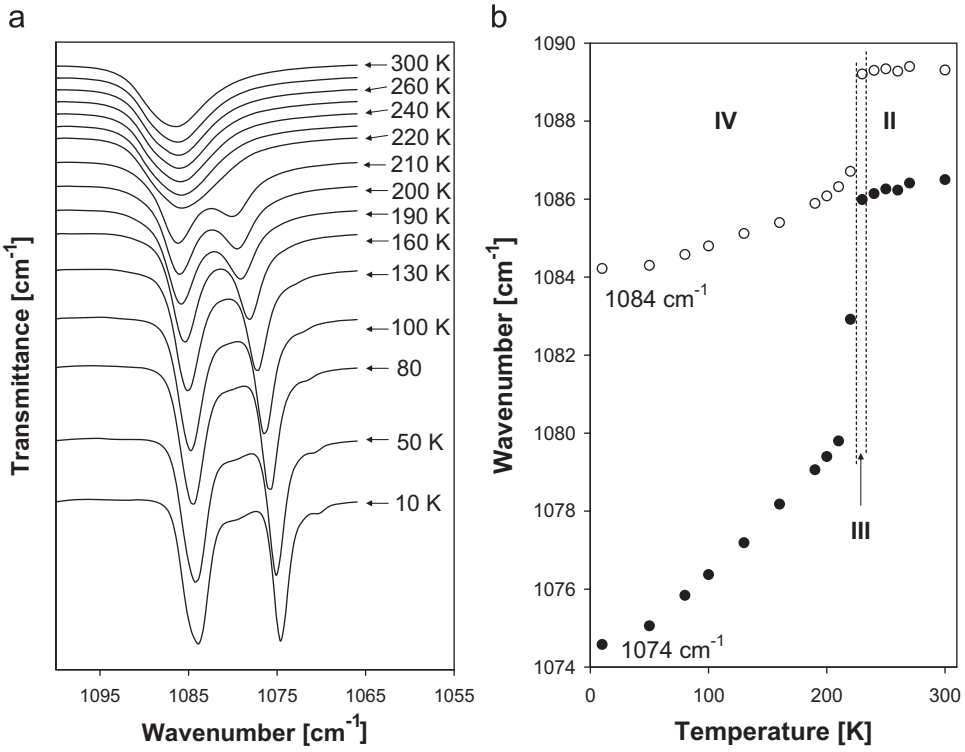

Fig. 13. (a) Temperature evolution of the IR spectra in the δ(C−H) modes vibrations region (1065−1095 cm^{-1}) and (b) temperature dependence of the wavenumber positions of the δ(C−H) modes (1074 and 1084 cm^{-1}).

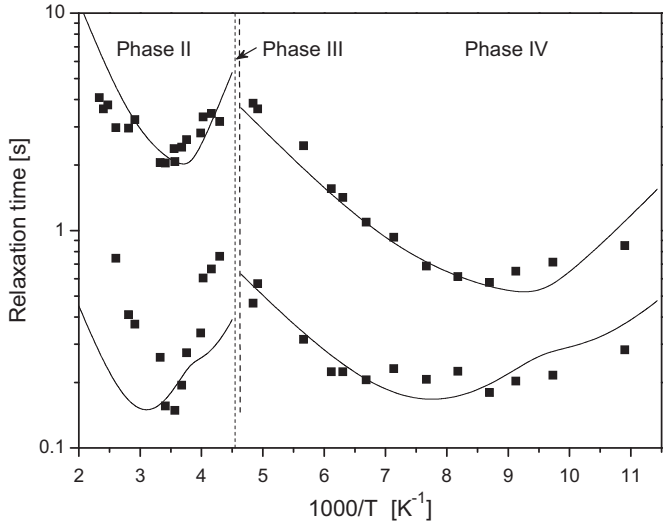

Fig. 14. Experimental proton relaxation times versus reciprocal temperature for $[C_3N_2H_5]_6[Bi_4Br_{18}]$ at 90 MHz and theoretical relaxation curves obtained as a least square fit in the lower temperature range (below 219.5 K) for $\tau_0 = 9.0 \times 10^{-12}$ s, $E_a = 4.0$ kJ/mol, $C^+ = 0.53$, $C^- = 0.32$ and as a result of calculations using $\tau_0 = 9.0 \times 10^{-12}$ s, $E_a = 10$ kJ/mol, $C^+ = 0.6$, $C^- = 0.085$ for higher temperatures (above 219.5 K). C^+ and C^- are explained in the supplementary material (Part D).

Bromide analogs in comparison to the chloride ones additionally undergo a high temperature PT (II→I). The isomorphism of these crystals is only partially reflected in their physical properties. The structural properties of the presented analogs appear to be similar only over the room temperature phases described by the same space group, $C2/m$. In all cases in this phase, three nonequivalent organic cations are orientationally disordered, but freezing of their motion at low temperatures proceeds differently. It was shown that imidazolium cations occupy the $C_s(2)$ sites (one carbon atom (C(2*A*), C(2*B*) or C(2*C*)) of each cation precisely lie in the C_s plane). Such a situation constrains disorder of the organic cations. Ceasing of the reorientational motion of the cations is expected to lead to loss of the symmetry plane and a change in the space group of these compounds. Unexpectedly, in the case of $[C_3N_2H_5]_6[Bi_4Br_{18}]$ the lowest temperature phase **IV** is described by the same space group, $C2/m$, as the phase **II**. On the other hand, these phases are separated by the intermediate phase **III**, for which the space group could not be determined. The powder X-ray diffraction studies suggest, however, that the phase **III** has some features characteristic of the surrounding phases.

The structural and dielectric studies of three crystals mentioned above proved that mobile organic cations bestowed significant dipole moments contribute principally to the complex electric permittivity of the system. Thus, the dynamics of the cationic framework of the analyzed compounds is well reflected in the dielectric response of the compounds. A static dielectric function gives information about the character of dipole–dipole interactions and a dielectric increment (strength of relaxators). Static dielectric characteristics of the imidazolium analogs are quite similar to each other. Both the electric permittivity value over the disordered phases ($C2/m$) and the step-wise anomaly of the permittivity at the transition temperature are comparable for the discussed compounds. However, the static dielectric response of $[C_5NH_6]_6[Bi_4Cl_{18}]$ in the vicinity of its PTs is distinctly different in comparison with those for the imidazolium ones. Ceasing of dipoles (polar pyridinium cations) proceeds continuously even at the phase transition temperatures. The most characteristic features which distinguish the pyridinium analogs from the imidazolium ones is the fact that ε is several times larger in the pyridium analogs and the dielectric anomaly showing a divergence of near the phase transition at 154 K to some extent resembles that encountered in typical ferroelectric materials. The comparison of the dielectric properties of the analyzed crystals leads to the conclusion that the dipole–dipole interactions are

dominant in $[C_5NH_6]_6[Bi_4Cl_{18}]$, whereas in the imidazolium analogs they are residual. A common feature of all three compounds is the presence of the dielectric relaxation processes. The dielectric dispersion studies of $R_6Bi_4X_{18}$-type compounds prove that the motion of the polar pyridinium cations is quite fast (the microwave frequency region), whereas for the imidazolium ones is rather slow (kilohertz frequency region). Nevertheless, the dielectric relaxation studies confirmed the motion of the cationic units for all analyzed compounds.

The value of the entropy change (ΔS_{tr}—39 J/mol K) accompanying the first order phase transition at 219.5 K for $[C_3N_2H_5]_6[Bi_4Br_{18}]$ and at 215 and 145 K for $[C_3N_2H_5]_6[Bi_4Cl_{18}]$ allows us to classify these transitions as an "order–disorder" type and the dynamics of the imidazolium cations is the main contribution to the mechanism of the phase transitions. The magnitude of (ΔS_{tr}) is large, however, it is distributed over six cations of the compound performing the jumps between two or three sites.

The mechanism of the phase transition in $[C_3N_2H_5]_6[Bi_4Br_{18}]$ governed by the dynamics of the cationic substructure seems to be consistent with the present vibrational properties of this compound. Significant changes in the IR spectra in the vicinity of 219.5 K may reflect a drastic change in the motional state of the imidazolium cations through the phase transition. It should be added that the bands assigned to the N−H···Br protonic stretching vibrations are highly sensitive to the IV→III or III→II PT, which indicates that the hydrogen bond system plays an important role in the dynamics of the organic cations.

In summary we would like to stress the point that reorientational disorder of the imidazolium cations over the phase **II**. The dynamics of cations is believed to contribute mainly to the phase transition mechanism at 219 K which was confirmed by the following experimental facts:

(i) large thermal displacement of atoms of the imidazolium rings disclosed by the X-ray diffraction,
(ii) a clear dielectric relaxation process ascribed to the motion of the dipolar imidazolium cations,
(iii) large transition entropy (ΔS_{tr}), which is undoubtedly related to the "order–disorder" mechanism of the phase transition,
(iv) ^{1}H NMR results clearly indicate the C_5'-type motion of the imidazolium cations over the phase **II**.

5. Conclusions

- The crystal structure of $[C_3N_2H_5]_6[Bi_4Br_{18}]$ consists of discrete $[Bi_4Br_{18}]^{6-}$ tetramers and disordered cations linked via very weak N−H···Br hydrogen bonds.
- DSC and dilatometric studies indicate the presence of two reversible phase transitions below room temperature: of first-order type: at 219/219.5 K (cooling/heating) with $\Delta S_{(II\rightarrow III)} = 39.3 \pm 6$ J/mol K and second-order at 227 K. The lower temperature transition may be classified as an "order–disorder" type. At high temperatures $[C_3N_2H_5]_6[Bi_4Br_{18}]$ undergoes an irreversible first-order transition at 410 K which modifies a phase transition sequence at low temperatures.
- A dielectric relaxation process disclosed over the phase **II** may be explained in terms of the motion of the dipolar imidazolium cations which appeared to be orientationally disordered.
- The infrared studies of the polycrystalline $[C_3N_2H_5]_6[Bi_4Br_{18}]$ showed that the ν(N−H), δ(ring) and δ(C−H) modes of the imidazolium cations appeared to be very sensitive to the low temperature phase transition IV→III.
- The ^{1}H NMR studies indicate that the bi-exponential proton magnetization decay in $[C_3N_2H_5]_6[Bi_4Br_{18}]$ may be caused by strong quadrupole interactions of the Br nuclei affecting the relaxation of protons through mutual H–Br dipole–dipole couplings.
- The results of the single crystal X-ray, thermal and used the spectroscopic methods lead to the conclusion that the structural phase transitions III→IV of the "order–disorder" type at 220 K is characterized by a complex mechanism. Its "order–disorder" contribution is believed to be associated mainly with the dynamics of the dipolar organic cations, whereas the "displacive" contribution is related to the mutual shift/deflection of the pentagonal rings.

Acknowledgment

This work was supported partially by the Polish State Committee for Scientific Research (Project Register: N N202 172 135 (PB 5.9)).

Appendix A. Supplementary data

Supplementary data associated with this article can be found in the online version at doi:10.1016/j.jssc.2009.08.007.

References

[1] L. Sobczyk, R. Jakubas, J. Zaleski, Pol. J. Chem. 71 (1997) 265.
[2] R. Jakubas, Solid State Commun. 60 (1986) 389.
[3] R. Jakubas, U. Krzewska, G. Bator, L. Sobczyk, Ferroelectrics 77 (1988) 129.
[4] R. Jakubas, A. Miniewicz, M. Bertault, J. Sworakowski, A. Ecolivet, J. Phys. France 50 (1989) 1483.
[5] J. Zaleski, A. Pietraszko, Acta Crystllogr. B 52 (1996) 287.
[6] R. Jakubas, Solid State Commun. 69 (1989) 267.
[7] P. Carpentier, J. Lefebvre, R. Jakubas, Acta Crystallogr. B 47 (1991) 228.
[8] J. Jóźków, R. Jakubas, G. Bator, A. Pietraszko, J. Chem. Phys. 114 (2001) 7239.
[9] R. Jakubas, A. Piecha, A. Pietraszko, G. Bator, Phys. Rev. B 72 (2005) 104107.
[10] A. Piecha, A. Pietraszko, G. Bator, R. Jakubas, J. Solid State Chem. 181 (2008) 1155.
[11] A. Piecha, A. Białońska, R. Jakubas, J. Phys. Condens. Matter 20 (2008) 325224.
[12] B. Aurivillius, C. Stälhandske, Acta Chem. Scand. A 32 (1978) 715.
[13] A. Piecha, R. Jakubas, A. Pietraszko, J. Mol. Struct. 844 (2007) 132.
[14] G.M. Sheldrick, Acta Crystallogr. A 64 (2008) 112.
[15] A.L. Rheingold, A.D. Uhler, A.G. Landers, Inorg. Chem. 22 (1983) 3255.
[16] A. Piecha, G. Bator, R. Jakubas, J. Phys. Condens. Matter 17 (2005) L411.
[17] J. Baran, G. Bator, R. Jakubas, M. Śledź, J. Phys. Condens. Matter 8 (1996) 10647.
[18] M. Cordes, J.L. Walter, Spectrochim. Acta 24A (1968) 237.
[19] L. Colombo, P. Bleckmann, B. Schrader, R. Schneider, Th. Plesser, J. Chem. Phys. 61 (1974) 3270.
[20] F. Billes, H. Endredi, G. Jalsovszky, J. Mol. Struct. (Theochem.) 465 (1999) 157.
[21] K. Fan, Y. Xie, J.E. Boggs, J. Mol. Struct. 136 (1986) 339.
[22] M. Majoube, G. Vergoten, J. Mol. Struct. 266 (1992) 345.
[23] M.A. Hooper, D.W. James, Aust. J. Chem. 26 (1973) 1401.
[24] M.H. Kuok, S.C. Ng, M. Iwata, Y. Ishibashi, Solid State Commun. 56 (1993) 151.
[25] J. Laane, P. Jagodzinski, Inorg. Chem. 19 (1980) 44.
[26] I. Belkyal, R. Mokhlisse, B. Tanouti, N.B. Chanh, M. Couzi, Phys. Status Solidi (A) 136 (1993) 45.
[27] A. Piecha, A. Białońska, R. Jakubas, W. Medycki, Solid State Sci. 10 (2008) 1469.